Interactions and reversal-field memory in complex magnetic nanowire arrays

Aurelian Rotaru, Jin-Hee Lim, Denny Lenormand, Andrei Diaconu, John. B. Wiley, Petronel Postolache, Alexandru Stancu, and Leonard Spinu

Phys. Rev. B **84**, 134431 — Published 20 October 2011

DOI: 10.1103/PhysRevB.84.134431

Interactions and Reversal-Field Memory in Complex Magnetic Nanowire Arrays

Aurelian Rotaru,[1,2] Jin-Hee Lim,[1,3] Denny Lenormand,[1,4] Andrei Diaconu,[1,4]
John. B. Wiley,[1,3] Petronel Postolache,[5] Alexandru Stancu,[5] and Leonard Spinu[1,4]

[1]*Advanced Materials Research Institute - AMRI, University of New Orleans, New Orleans, LA 70148, USA*
[2]*Faculty of Electrical Engineering and Computer Science, "Stefan cel Mare" University, Suceava 720229, Romania*
[3]*Department of Chemistry, University of New Orleans, New Orleans, LA 70148, USA*
[4]*Department of Physics, University of New Orleans, New Orleans, LA 70148, USA*
[5]*Department of Physics, Faculty of Physics, "Alexandru Ioan Cuza" University, Iasi 700506, Romania*

Interactions and magnetization reversal of Ni nanowires arrays have been investigated by the first order reversal curve (FORC) method. Several series of samples with controlled spatial distribution were considered including simple wires of different lengths and diameters (70 nm and 110 nm) and complex wires with single modulated diameter along their length. Subtle features of magnetic interactions are revealed through a quantitative analysis of the local interaction field profile distributions obtained from FORC. In addition the FORC analysis indicates that the nanowire systems with a mean diameter of 70 nm appear to be organized in symmetric clusters indicative of a reversal-field memory effect.

PACS numbers: 75.60.-d, 75.60.Ej, 81.07.Gf

I. INTRODUCTION

Magnetic nanowires are an important class of magnetic nanostructured materials[1–3]. Due to size confinement, new phenomena arise in these systems which makes them ideal candidates for important technological applications in spintronics and as microwave devices[4–9], high-density recording media, and permanent magnets[10]. For the above mentioned applications as well as for fundamental studies of magnetic interactions and magnetization reversal in model systems, the most useful configuration is a periodic array of nanowires where the size of the components and their reciprocal arrangement can be controlled. One of the most versatile methods of preparing periodic arrays of magnetic nanowires is the use of nanometer-sized templates where the wires are grown by electrodeposition techniques. This method has advantages over the standard preparation methods of nanowires by lithographic approaches. First of all, the template method of growing nanowires is not as laborious and does not require as sophisticated of instrumentation as in electron-beam lithography. Further, the approach readily allows fabrication of large size samples and is a unique way to obtain volumetric arrays of magnetic nanowires as opposed to the planar arrangements common to other methods. There are several nanoporous materials that can be used as templates but the most common for unidimensional nanostructures are anodic porous alumina and track-etched polymer membranes[11,12]. These membranes allow fabrication of uniform arrays of metallic nanowires with large aspect ratios over a large range of wire diameters and interwire distances.

The strength of magnetic interactions in magnetic nanowire arrays can be controlled effectively by varying the interwire spacing. The spacing provided by the polymer membranes is difficult to control due to the randomness of pore location obtained through the combination of the charged particle bombardment (irradiation) and chemical etching[12,13]. In spite of recent progress in fabrication of ion track nanochannels that allows a better control of the number of the pores in a membrane, their precise location is still problematic[14]. Conversely, templates obtained by aluminum anodization provide for better control of the pores through a combination voltage, acid concentration and time used during the oxidation process[12]. Moreover, through a multistep anodization scheme one can obtain alumina membranes with more complex configurations that can be used to prepare nanowires with modulated diameters and/or varying interwire distances[15]. The advantage of this approach is the ability to obtain membranes with different average distances between pores while preserving the same diameter distribution[16].

One of the most important effects in magnetic nanowire arrays is the interwire magnetostatic interactions[17–22]. The interwire interaction significantly affects magnetic properties of magnetic nanowire including magnetization switching[21,23], microwave[17,24] and magnetotransport properties[5,8]. Consequently, in order to understand the obtained experimental results, reliable methods for interactions evaluation are needed. To quantify the effect of interactions one needs both a suitable method to experimentally vary the strength of interactions in arrays of magnetic nanowires and a method to measure the effect of the interactions.

Any experimental method used to quantify the interactions in magnetic systems must be simple to implement by starting from a reproducible and easy to achieve initial state, by requiring a reasonable number of measurement points and by providing, directly or after some preferably simple data processing, a meaningful parameter characterizing the strength of interactions. For ferromagnetic

materials the major hysteresis loop (MHL) is the distinctive fingerprint and the simplest measurement protocol, obtained by cycling the applied magnetic field (input) and recording the ensuing change of magnetization (output) of the specimen along the field direction. Unfortunately, through its main parameters coercive field, remanent and saturation magnetizations, MHL cannot provide an adequate description of magnetic interactions. In spite of some attempts to consider more subtle features of the MHL as its shape (squareness, shear, etc.)[25,26], it proved not to be a suitable alternative to quantitatively characterize magnetic interactions, situation stemming from exactly MHL's main advantage, simplicity. More complex magnetization curves covering states with field and magnetization values located inside the MHL, as higher order magnetization curves[27,28], can give additional information that can be used for magnetic interaction characterization. The term high order is meant to underline the fact that each magnetization curve is obtained after a number of reversals of the input, i.e. magnetic field[28]. Thus, the MHL is considered a zero order magnetization curve whereas any magnetization curve obtained after the field variation sign is reversed at a certain point of the MHL is of first order, reversed twice, second order, and so on. To be more specific, if we start from the positive saturation of the sample, when the field is decreased we are measuring the descending branch of MHL (zero order curve). If at a certain value of the applied field (not sufficient to saturate the sample in the negative sense) the field is increased, a first order curve will be measured. Analogously, if at a certain value of the applied field one starts to decrease the field instead of continuing increasing it towards the positive saturation one measures a second order magnetization curve and the same technique can be used to obtain higher order curves. Several high order magnetization protocols were proposed to probe the effect of interactions in assembly of magnetic particles as Henkel Plots[29], deltaM-plots[30], and First Order Reversal Curves (FORC)[28,31,32]. The first two methods offer only a qualitative evaluation of magnetic interactions starting from a relation established by Wohlfarth between the different modes of acquisition of remanent magnetization of non-interacting ferromagnetic particles[33], i.e. isothermal remanent magnetization (IRM) and DC demagnetization. In addition, the results obtained using these methods are not very stable being dependent on the manner used to obtain the demagnetizing state prior the IRM measurements[34]. First Order Reversal Curves, introduced by Mayergoyz as an identification method for Preisach Model[31], were proposed by Pike as a better alternative than deltaM-plots for studying magnetic interactions in assemblies of magnetic entities[32]. First, by decreasing the order of the employed magnetization curves to one, experimentally the FORC method is simpler to implement. Second, the initial state for every FORC-type measurement is the magnetic saturation which is highly reproducible and easy to achieve. Finally, from the First Order Reversal Curves, following a well-defined transform, the FORC distribution is obtained which can be used to characterize the interactions and magnetization reversal in hysteretic systems. The FORC distribution and/or FORC diagram which is obtained as a contour plot of the former, offer qualitatively visual information on the interaction in a system that can be easily used to differentiate systems with different interaction strengths. Further, through the values of FORC distribution parameters, this method provides a quantitative assessment of interaction which is not affected by the problems of delta-M and Henkel plots mentioned above.

Soon after it was proposed, FORC method became an important experimental approach for interaction evaluation in hysteretic systems for a wide class of different materials ranging from magnetic[35–42] and electric[43–45] to spin transition systems[46–49]. In the case of magnetic nanowire arrays, Spinu et al.[37] proposed for the first time FORC as an effective method for magnetic interactions characterization with many other reports following[50–56]. In the majority of these reports the FORC method was used mostly as a qualitative tool to picture the existence of interaction and coercive distributions without a comprehensive quantitative analysis of magnetic interactions. One of the reasons for this situation was the lack of a series of samples with tuned interaction strengths and predetermined morphological parameters that can facilitate a correct and coherent interpretation of the wealth of information provided by the FORC measurements via theoretical models. In fact, one of the advantages of using templates for magnetic systems fabrication is the possibility of obtaining model systems that can be used to test the validity of theoretical models. As the quality of materials is dependent on the morphology of the templates, an accurate interpretation of the experimental results is difficult, especially for templates with a large geometric variability as it is the case of commercially available templates used exclusively on all previous FORC studies on magnetic nanowire arrays.

In this study, by a combined sample design and experimental measurements approach we quantitatively analyze the effect of magnetic interactions and investigate the magnetization reversal in highly-ordered magnetic nanowire arrays. The magnetic nanowires were grown in highly-ordered anodic alumina membranes for which the spatial distribution of the pores was controlled by a sequential application of mild and hard anodization techniques[16]. Several series of samples were considered including simple wires of different lengths and diameters (70 nm and 110 nm) and complex wires with single modulated diameter along their length. The FORC method was used to quantify the effect of magnetic interactions in the series of magnetic nanowire arrays. Besides the qualitative investigation of FORC diagrams, more subtle features of magnetic interactions in complex wires are revealed through a quantitative analysis of the profile of the local interaction field distributions. In addition, the FORC analyses indicate that the nanowire systems with

a mean diameter of 70 nm appear to be organized in symmetric clusters indicative of a reversal-field memory effect[57].

II. EXPERIMENTAL

A. Sample Fabrication

Here we focus on Ni wires deposited in anodic aluminum oxide (AAO) membranes. The membranes were prepared by either a two- or three-step anodization procedure[16]. To prepare the standard Mild AAO (Mi-AAO) membranes by the two-step method, first an Al film with a thickness of 0.25 mm was annealed at 450 °C for 5 h in Ar atmosphere, then the sample was electropolished in a 1:4 (volume ratio) solution of perchloric acid-ethanol at 25 V, 10 °C before anodization in 0.3 M oxalic acid at 40 V, 17 °C. After the oxide layer was removed at 80 °C in a solution of 1.8 wt% chromic acid-5 wt% phosphoric acid, a second anodization was performed in oxalic acid resulting in Mi-AAO. To prepare more complex membranes with larger interpore distances, the same anodization procedure as described above for Mi-AAO was carried out, but with an additional anodization step (hard condition) at 100 V for 30 min at 5 °C to produce the Mi-Ha AAO. After the second or third anodization steps, templates were detached from the Al film by an electrochemical treatment in 1:1 mixture solution of perchloric acid-ethanol at 100 V at 10 °C. The samples were then rinsed with distilled water and acetone. To completely remove the barrier layers, samples were immersed in a 5 wt% phosphoric acid solution. An example of such membranes prepared by multistep anodization is shown in Fig. 1. In the transition from the mild region to the hard region, approximately half of the channels remain continuous throughout the membrane while other pores initiated on the mild side terminate at the mild-hard interface. The Mi-Ha AAO can be employed as a membrane for the fabrication of the magnetic nanowires arrays. Wires were grown either in the hard or mild side of these membranes. In the hard side of the membrane, 110 nm diameter wires are readily obtained within all available pores. Wires fabricated in the mild side of the AAO template, however, only grow in selected pores.

Ni nanowires were grown in the pores of AAO templates by electrodeposition. Initially an Ag film was sputtered onto one side of AAO template. Metal nanowires were then grown over several minutes at room temperature by a constant current method at 0.5 mA on a Princeton Applied Research VMP2 with a Pt wire counter electrode. A commercially available Ni plating solution (Technics Inc., Nickel sulfamate-RTU) was used. Synthesized nanostructures were characterized by field-emission scanning electron microscopy (FESEM) on a LEO 1530 VP. Nanowires of different lengths were prepared by simply varying the electrodeposition time.

In this work, we have selected 4 sets of nanowire arrays for a total of 12 in order to study the effect of the diameter, the length and interpore distance on the magnetic properties of single-diameter nanowire arrays. Also, we studied magnetic properties of single modulated diameter nanowire arrays, where each nanowire has two different diameters. The four sets of samples are represented schematically in Fig. 2. The samples labelled Mild (Mi) are array of nanowires deposited in the pores of the membrane obtained through a single step mild anodizing process, characterized by diameters of 70 nm, with an interpore distance of 100 nm. The Mild-Hard (Mi-Ha) samples are nanowires deposited only in the mild side of Mi-Ha templates. The mean diameter of the nanowires is 70 nm, and the interpore distance is about 250 nm. The Hard-Mild (Ha-Mi) nanowires were deposited only in the hard side of Mi-Ha templates obtaining wires with a mean diameter of 110 nm and an interwire distance of 250 nm. The Single Modulated (SM Mi-Ha) templates are identical to Mi-Ha and Ha-Mi, but here wires are grown such that they cross the mild and hard interface, starting from the mild side, to produce single modulated diameter structures. In this case, the portion of the nanowire from the mild side is always 14 μm in length and 70 nm in diameter, while the portion from the hard side has various lengths with a diameter of 110 nm.

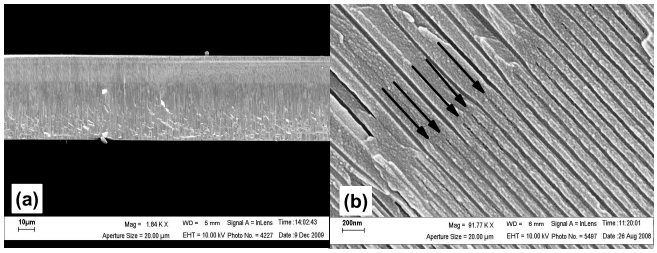

FIG. 1. FESEM images of Mi-Ha AAO template. (a) Cross section of the boundary of mild (top) and hard (bottom) side. (b) Higher magnification view of boundary region of Mild (bottom–right) and Hard side (top-left); black arrows highlight some selected pores that have been terminated on the hard anodization side.

B. Magnetic measurements

The magnetic measurements (major hysteresis loops (MHL) and FORCs) were done at room temperature on a Princeton AGM-VSM Magnetometer (using the VSM option); this instrument is able to record a set of 100 FORCs in less than 2 hours. The FORC measurement begins with a positive saturation of the samples followed by a ramping down of the applied field to a reversal field H_r. Then the field is increased again up to saturation and magnetization is measured at different values of the applied field H. Thus, for different values of the reversal field H_r a family of FORCs is obtained with $M(H, H_r)$ representing the magnetization obtained in the applied field H after a field reversal at H_r. A typical family of

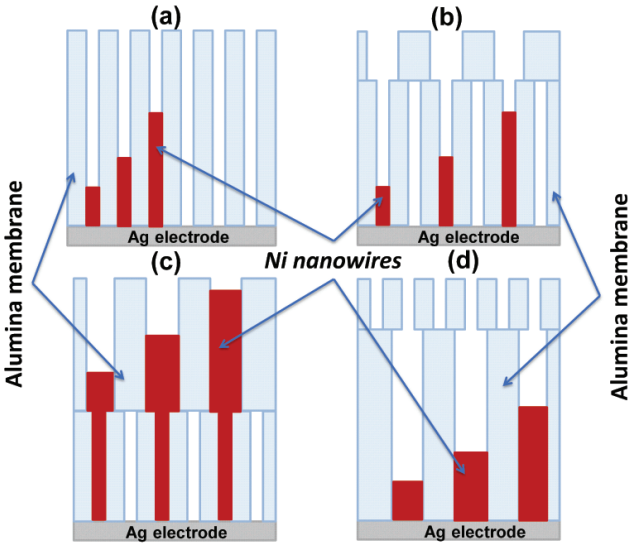

FIG. 2. Schematic representation of the four series of samples considered (a) Mi, (b) Mi-Ha, (c) Single Modulated SM Mi-Ha and (d) Ha-Mi. Each series has three samples: each sample contains nanowires of constant length, the length being different from sample to sample. The individual samples within each series are represented schematically by the three wires of different lengths in each figure, (a), (b), (c) and (d).

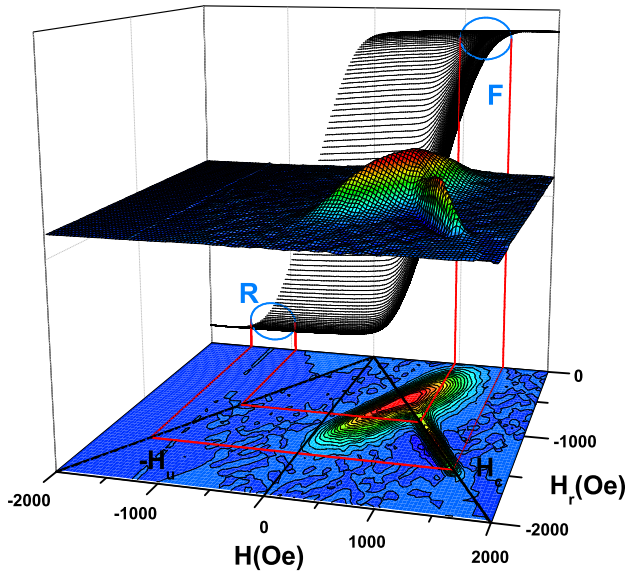

FIG. 3. (Color online) A family of FORCs from the Mi-Ha-4.8 μm nanowire array (vertical-back panel), the corresponding FORC 3D distribution (top horizontal panel) and FORC diagram (bottom horizontal panel).

FORCs is shown in the vertical-back panel of Fig. 3 for Mi-Ha-4.8μm sample (70 nm diameter nanowires, interwire distance of 250 nm, and length of 4.8 μm). In all measurements the magnetic field was applied along the length of the nanowire. The FORC distributions were obtained by computing the mixed second order derivative of magnetization $M\left(H, H_r\right)$:

$$\rho(H, H_r) = -\frac{1}{2}\frac{\partial^2 M}{\partial H_r \partial H} \tag{1}$$

using a numerical interpolation algorithm. Specifically, the FORC distributions and diagrams (the contour plots of the FORC distributions) were produced using FORCinel, an algorithm using locally weighted regression smoothing[58]. The FORC distribution as a 3D plot and FORC diagram as 2D contour plot in coordinate (H, H_r) for sample Mi-Ha-4.8μm are represented in the top and bottom horizontal panels of Fig. 3, respectively.

Usually a new set of coordinates (H_c, H_u) are defined with $H_c = \left(H - H_r\right)/2$ and $H_u = \left(H + H_r\right)/2$, which rotates the FORC distribution by 45° as seen in the bottom horizontal panel of Fig. 3. Further, the FORC diagram is shown as a contour plot in the (H_c, H_u) plane with horizontal coercivity axis H_c and vertical interaction axis H_u (see Figs. 4, 5).

In order to quantitatively compare different FORC diagrams obtained for different samples, a statistical analysis was carried out of the profiles of both interaction and coercive field distributions. Hence, the distribution parameters as mean field values of coercive, $\langle H_c \rangle$, and interaction fields, $\langle H_u \rangle$, and their corresponding standard deviations, σ_{H_c}, σ_{H_u} were obtained[46]. The parameters for all samples considered in this study are given in Table I.

III. RESULTS AND DISCUSSION

A. Study of the Interactions

The main advantage of the use of the AAO templates is the fact that they allow, while keeping the same diameter distribution, the modification of the interpore distance through a controlled obstruction of the pores. In this section we study and compare the magnetic properties of the systems Mi-AAO vs. Mi-Ha AAO. The difference between these two systems is the average pore-pore distance. The Mi-AAO systems are characterized by a nominal diameter of 70 nm, with a mean interpore distance of 100 nm, being synthesized with three different nominal lengths: 4.0 μm, 9.0 μm and 15.0 μm. The second system, Mi-Ha AAO, is characterized by the same nominal wire diameter of 70 nm, but with a mean interpore distance of about 250 nm; wires were fabricated

with three different lengths: 4.8 μm, 8.5 μm and 15.8 μm respectively.

For these ranges of diameters and lengths of the Mild and Mi-Ha nanowires the demagnetizing factor of the wires do not vary significantly[59] and, as expected, within the same series, Mi or Mi-Ha, the FORC diagrams do not display any noticeable variation as a function of the length of the nanowires. In Fig. 4a) and Fig. 4b) are displayed the corresponding normalized FORC diagrams for the Mi-Ha and Mild nanowires with a length of 8.5 μm and 9.0 μm, respectively. The top and the side insets represent the local coercive and interaction field distribution profiles obtained as horizontal and vertical cross-sections, respectively, of the FORC distribution through its main maximum. One observes that as the interwire distance decreases the standard deviation of interaction field distribution, σ_{H_u}, increases more than two times, while the most probable value and standard deviation of coercive field distribution varies only slightly (see Table I). This is a clear indication of the increased effect of interwire interaction as only the distance between nanowires is decreasing. In the majority of previously published studies of interacting magnetic nanowires it was difficult to isolate and evaluate the effect of interactions as comparing different samples because more than one parameter of the assembly was varied, not just the interactions.

As shown in Fig. 4 a) and c), by comparing the dispersion of interactions in Mi-Ha and Ha-Mi samples one observes that for the same interpore distance of 250 nm the strength of interwire interactions is larger for the Ha-Mi sample (110 nm in diameter) than for the sample Mi-Ha (70 nm). As shown in Table I, one observes that the standard deviation of the local interaction field, σ_{H_u}, in all Ha-Mi samples has about the same value as in the corresponding Mild samples for the three lengths considered in this study. In fact, by increasing the nanowire diameter, while the distance between their centers remains constant, the mean interaction field is also increasing, due to the closer proximity of the wires' walls (180 nm (Mi-Ha) vs. 140 nm (Ha-Mi)). Regarding the coercive field distribution of the FORC diagrams in Fig. 4, one observes a slight increase of the average coercive field value, $\langle H_c \rangle$, for Mild sample relative to the Mi-Ha one while a horizontal ridge is present in the FORC diagrams of both samples. The origin of this "tail" of the FORC diagram is related to the switching mechanisms in the arrays of magnetic nanowires and will be discussed in the next section.

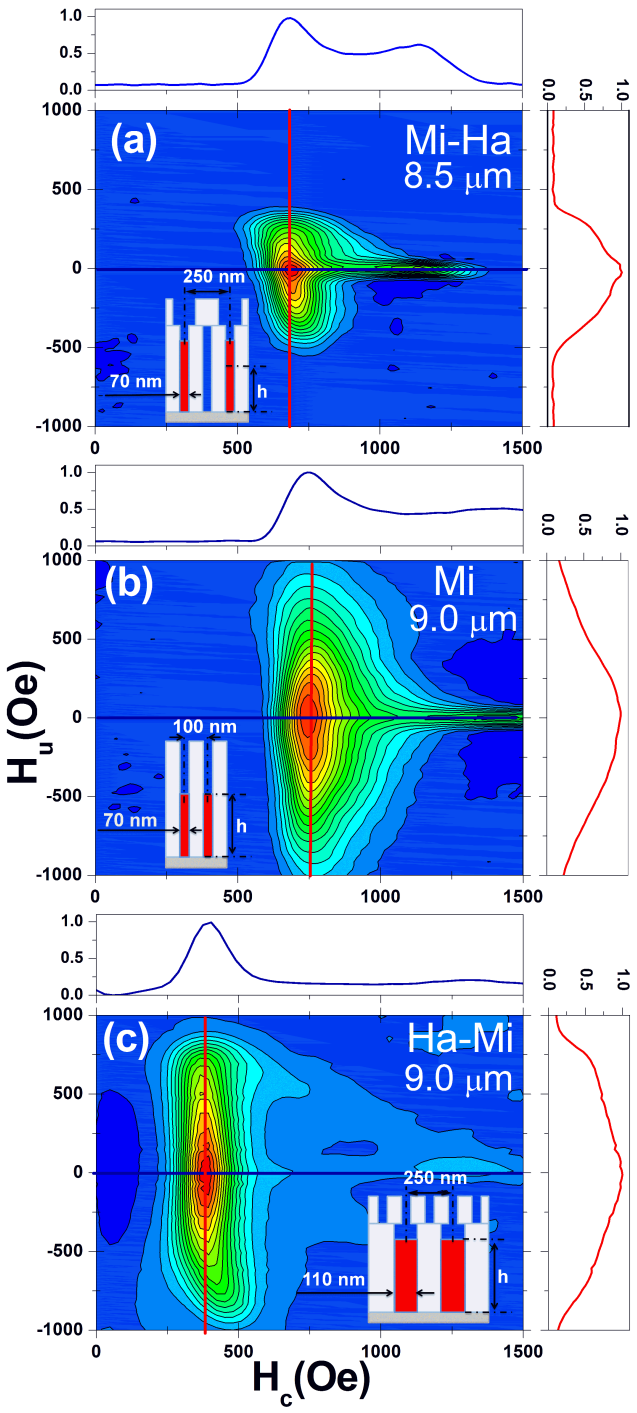

FIG. 4. (Color online) FORC diagrams of 8.5 μm-long Mi-Ha nanowire array (a) 9 μm-long Regular Mi nanowire array (b) and 9 μm-long Ha-Mi nanowire array (c). The top and the side insets for each figure represent the coercive field and interaction field distribution profiles obtained at the location of the horizontal (blue color online) and (red color online) vertical lines, respectively. The values of diameters and center-to-center interwire distances are given for each sample in the corresponding diagrams.

B. Reversal-field memory effect

The appearance of this horizontal ridge along the coercive field axis has been reported in the literature[50]. Béron et al. suggested that the origin of this tail in FORC diagrams is due to a nonuniform length distribution such that during the magnetization process, the system acts as two populations of magnetic entities[50].

They tested this assumption by polishing the top of a wire membrane, after which the horizontal ridge in the FORC diagram disappears. In order to verify the same hypothesis on our nanowire arrays we considered single modulated diameter Mi-Ha nanowires (SM Mi-Ha) presenting two different diameters, 70 nm and 110 nm. Nanowires were grown in Mi-Ha AAO template starting from the Mild side (diameter 70 nm), filling completely the Mild side and continuing partially into the Hard side. From Fig. 1(a) one observes that the separation between the Mild side and Hard side is very uniform which determines a very variation of the Mild side section length of the SM Mi-Ha nanowires. The FORC diagrams of all single modulated diameter nanowire arrays display the horizontal ridge along the coercivity axis (see Fig. 5). The horizontal ridge is not the result of the larger diameter section in the composite wires because no ridge was observed for any of the samples with large diameter Ha-Mi as shown in Fig. 4. Consequently, in our case the origin of the horizontal ridge in the FORC diagram is not the result of an irregularity in the system, as length variation, but merely an intrinsic characteristic of small diameter nanowires.

The ridge along the coercivity axis, i.e. a wide range of coercivities with a narrow range of interactions, is in fact an additional irreversible FORC distribution located at large H_c values and very small interaction field H_u values ($H_u \simeq 0$). To get a better insight into the origin of the horizontal ridge in smaller diameter nanowire arrays we should refer to Fig. 3 where the FORC diagram is represented in the original coordinates (H, H_r), where $H = H_u + H_c$ and $H_r = H_u - H_c$ (see Section II B). Thus, in terms of (H, H_r) coordinates one can easily observe that the ridge is determined by switching events occurring at large values of the applied field H after a reversal field $H_r \simeq -H$. In Fig. 3 this property of the ridge appears evident by projecting from magnetization curves FORC regions located at $H_r \simeq -H$ and H, (regions delimited by the blue ellipses "R" and "F", respectively) and observing that both these projections converge on the FORC diagram ridge. In other words, the ridge is the result of switching events occurring after a reversal in the "R" region and finishing in the "F" region of the M vs. H First Order Reversal Curves. These kind of switching events are consistent with the "reversal-field memory" effect observed by Katzgraber et al.[57] in Edwards Anderson Ising Spin Glass (EASG) Ising-type systems. The physical origin of the reverse-field memory effect was ascribed to the existence in the magnetic system of a significant proportion of symmetric hysterons. Hysterons are independent two-state switching units that change their states from +1 to -1 and from -1 to +1 at the fields $H_u - H_c = H_r$ and $H_u + H_c = H$, respectively. A symmetric hysteron has a bias field $H_u = 0$ and consequently switches "symmetrically" at H and $H_r = -H$. The presence of a distribution of symmetric hysterons is evidenced by a kink in the magnetization curve, which is reflected in the FORC diagram as a ridge with its extension proportional to the range of coercive field, H_c.

It was claimed by some authors (e.g. Ref. 23) that the magnetic nanowire arrays can be considered as a very good example of physical system correctly described by a Classical Preisach Model (also named CPM system). However, as Mayergoyz has shown in Ref. 28, the necessary and sufficient conditions to be obeyed by a CPM system are the wiping-out and congruency properties. Systematic studies show however that the nanowire systems do not satisfy the congruency property. This is certainly motivated by the mean field interactions that have to be taken into account in such systems. However, a comparison of the parameters obtained directly from the experimental FORC distributions can be performed and may indicate with some degree of accuracy the "real" Preisach distribution characteristic to various samples. A more accurate study will include the evaluation of the influence on the results due to the state dependence of the interaction field distribution and will be presented in a further paper.

Consequently, we consider for the moment that the nanowire systems are characterized by the Preisach distributions of hysterons $P(H_c, H_u)$, which are identical with the experimental FORC distributions $\rho(H_c, H_u)$. From the FORC diagrams obtained in the case of our nanowire arrays, one observes the presence of the horizontal ridge in the range of reversal field values $-800 \leq H_r \leq -1500$ Oe for the Mi-Ha AAO nanowire arrays and in the range of $-1100 \leq H_r \leq -1700$ Oe for regular Mi-AAO nanowire arrays respectively. However, as shown in Fig. 4 for the nanowire arrays with a larger diameter, Ha-Mi, the tail of the FORC diagram is drastically diminished if not negligible. Consequently, the presence of the reversal-field memory effect in the Mi-Ha samples, with small diameter, suggests that these samples have an important number of symmetric hysterons. In contrast, the absence of the reversal-field memory effect in the Ha-Mi samples indicates that if symmetric hysterons do exist, their proportion is not significant and the horizontal ridge in the FORC diagram is not present.

C. Magnetic properties tuning. Complex nanowire arrays.

We have seen in the previous section that the magnetic properties of Mi-Ha AAO arrays are quite different from those of Ha-Mi AAO arrays, especially the strength of dipolar interactions. A simple way to obtain magnetic nanowire arrays with intermediate magnetic properties is to combine the Ha-Mi and Mi-Ha nanowires within the same assembly to synthesize a single modulated diameter nanowire array. The magnetic properties of these complex nanowires can be further tuned by varying the length ratio of the two components, Mi-Ha and Ha-Mi. An exemplification of this approach is shown in Fig. 5 where are represented the FORC diagrams of Mi-Ha-15.8μm, Ha-Mi-15.0μm and modulated Mi-Ha-30μm composed of

two 15.0 μm long sections of diameters 70 nm and 110 nm. From the local interaction field distribution profiles shown in the right side panel one observes that the strength of dipolar interaction in the single modulated diameter nanowire array sample is intermediate between interactions in Mi-Ha and Ha-Mi samples. Furthermore, one observes subtle differences in the way the interaction field is decaying on moving away from the $H_u = 0$ line. Thus, in the Mi-Ha sample the dipolar interactions are localized with a quasi-linear decay of the interaction field, while in the Ha-Mi sample the interaction field is broadly distributed with a convex decay. The combination of the two aforementioned effects in the single modulated diameter nanowire samples results in an intermediate width of the interaction field distribution with a localized convex decay.

The statistical analysis done on the profiles of the interaction and coercive field distributions for all samples allows us to better assess and summarize these differences between samples from the three different series. For the sake of consistency the coercive field profiles $\rho(H_c)$ were fitted for all samples with a double-peak Gaussian distribution

$$\rho(H_c) = \sum_{i=1,2} A_i \exp\left[-\frac{(H_c - \langle H_{c,i}\rangle)^2}{2\sigma^2_{Hc,i}}\right] \qquad (2)$$

allowing determination of the average values $\langle H_{c1}\rangle$, and $\langle H_{c2}\rangle$ of coercive field for both peaks, and their corresponding standard deviations σ_{Hc1} and σ_{Hc2}. The same procedure was applied to the interaction field profiles $\rho(H_u)$ taken for each sample at $H_c = \langle H_{c1}\rangle$ and $H_c = \langle H_{c2}\rangle$. Using the standard deviations of the coercive and interaction field distributions for both peaks one calculated, $m_1/(m_1+m_2)$, the ratio between the magnetic moment associated with the lower coercivity peak, m_1, and the total magnetic moment m_1+m_2. As shown in Table I $m_1/(m_1+m_2)$, is very close to 100% for all Ha-Mi samples with large diameter (110 nm). For smaller diameter samples (Mi and Mi-Ha) the second FORC distribution peak is more noticeable as attested by smaller values of $m_1/(m_1+m_2)$. Essentially, for these samples the second distribution peak is part of the reversal field memory ridge discussed in the previous section, but depending on the interaction strength, one observes subtle differences. For Mi-Ha samples with weak dipolar interactions the second coercivity peak is well defined, while for Mi samples with stronger interwire interactions, the peak is absorbed in the horizontal ridge (see Fig. 4). Thus, the increase of interwire interactions has as an effect a delocalization of the symmetric hysteron distribution along the coercive field H_c axis.

For a better visualization of the statistical analysis results summarized in Table I, we plotted in Fig. 6 the length dependency of the main statistical parameters, average coercive field and dispersion of dipolar interaction field. One observes that for all series the average coercive field does not vary significantly with the length of

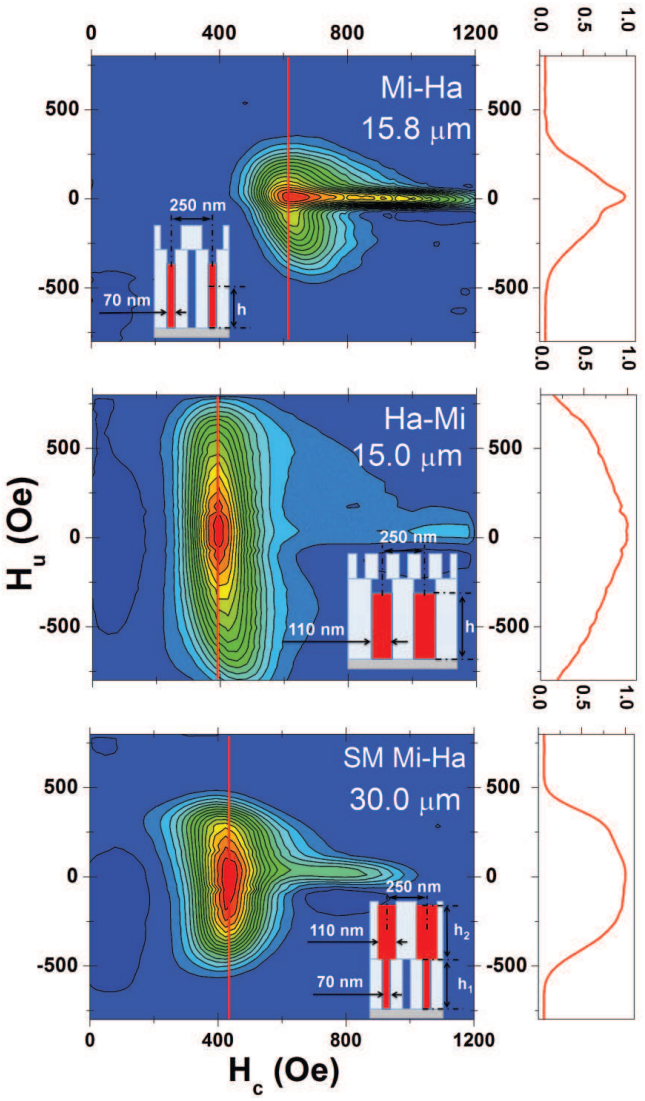

FIG. 5. (Color online) Comparison between FORC diagrams of Mi-Ha nanowire array (top), Ha-Mi AAO nanowire array (middle) and Single Modulated SM Mi-Ha nanowire array with the lengths of Mi and Ha segments h_1=15 μm and h_2=15 μm, respectively (bottom). The right side panel displays the corresponding profile of the local interaction field distribution for each sample. The values of diameters and center-to-center interwire distances are given for each sample in the corresponding diagrams.

nanowire within this length range. By increasing the wire diameter one observes a variation of the coercive field mean value from about 750 Oe, for a nanowire diameter of 70 nm (Mi samples), down to 400 Oe, for a diameter of 110 nm (Ha-Mi samples). This is consistent with a variation of the coercive field inverse proportional with the diameter previously observed in similar systems[60] and associated with a non-coherent magnetization reversal in the case of magnetic nanowires with diameter larger than the critical diameter D_{coh} which for Ni is 26 nm[61–63]. From the σ_{Hu} vs. wire length plot, it clearly appears

TABLE I. Statistical analysis of the FORC distributions.

Sample	$\langle H_{c1}\rangle$ (Oe)	$\sigma_{Hc1}(Oe)$	$\langle H_u\rangle$ (Oe)	σ_{Hu} (Oe)	$\langle H_{c2}\rangle$ (Oe)	σ_{Hc2} (Oe)	$m_1/(m_1+m_2)$ (%)
Mi-4μm	714	86	1	499	1302	465	86.0
Mi-9μm	764	87	-49	498	1313	358	85.5
Mi-15μm	740	79	-6	416	1261	389	82.5
Mi-Ha-4.8μm	670	87	-35	277	1090	200	83.0
Mi-Ha-8.5μm	720	92	-15	209	1080	181	79.9
Mi-Ha-15.8μm	617	77	-17	182	933	193	62.2
Ha-Mi-4μm	390	77	17	438	1259	117	98.1
Ha-Mi-9μm	390	70	16	548	1288	141	97.4
Ha-Mi-15μm	400	72	27	460	1144	171	96.5
Mi-Ha-(14+5)μm	488	74	-19	350	860	204	92.8
Mi-Ha-(14+10)μm	482	75	-29	340	867	210	91.8
Mi-Ha- (14+16)μm	436	80	-23	309	766	146	90.4

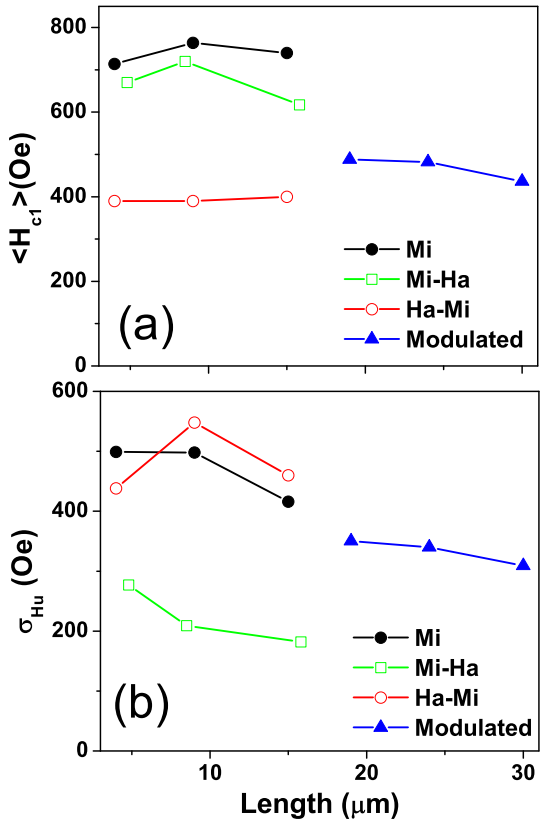

FIG. 6. (Color online) Length dependecy of (a) the mean value of the main coercive field, and (b) standard deviation of the main interaction field distribution

that the strength of interactions in complex nanowires is intermediate between the interactions in Mi-Ha and Ha-Mi samples, as discussed previously. Furthermore, by increasing wire diameters it is possible to strengthen the dipolar interactions arriving to the point that thick Ha-Mi wires have essentially the same value of the standard deviation of the interaction field as thin Mi wires. As the wire diameter is proved to be efficient for changing both the standard deviation of the interaction field distribution and the average wire coercivity, it is interesting to observe the properties of complex wires (thin + thick). The results show that these wires provide average values for both coercivity and interaction intensity which is another essential tool to obtain systems with tailored properties.

IV. CONCLUSIONS

We have systematically studied the dipolar interaction effects and reversal behavior in highly-ordered magnetic nanowire arrays by a combination of sample design and fabrication and magnetic measurements using the FORC method. Taking advantage of high quality AAO templates obtained through a sequential application of mild and hard anodization techniques we were able to include in our study four different series of nanowire samples with good control of diameter, interwire spacing and complexity (simple and single modulated diameter wires). The effect of dipolar interactions was studied by considering samples with virtually identical diameter distributions but different interwire distances as provided by a controlled obstruction of the pores of the AAO templates. This is essential for a correct evaluation of the effect of the interactions in magnetic nanowire arrays, as it is well known that nanowire arrays of with different diameters are subject to different strengths of interaction. Utilizing the FORC technique and through a quantitative analysis of the profiles of local interaction and coercive field distributions a detailed description of the magnetic interactions and magnetization reversal was obtained. Thus, for the Mi-Ha series with nanowires of 70 nm diameter and 250 nm interwire distance, the strength of dipolar in-

teractions was significantly reduced relative to nanowires from Mi series having the same diameter but a 100 nm interwire distance. In addition FORC analysis indicates that the nanowire systems with a mean diameter of 70 nm seem to be organized in symmetric clusters indicative of a reversal-field memory effect. The increase of interwire interactions enhances the reversal-field memory effect as reflected by a delocalization of the symmetric hysteron distribution towards higher coercive field values for the Mi samples. The Ha-Mi series including thick wires of 110 nm diameter and the same wire center-to-center distance as Mi-Ha series (250 nm) displayed an enhanced strength of interactions as in the case of Mi series. The composite Mi-Ha series composed of single modulated wires (70 nm and 110 nm) allowed us to obtain magnetic properties intermediate of those of simple thin and thick wires. Moreover, one observes subtle differences in the profiles of interaction field distributions. Thus, in the Mi-Ha sample the dipolar interactions are localized with a quasi-linear decay of the interaction field, while in the Ha-Mi sample the interaction field is broadly distributed with a convex decay. The combination of the two aforementioned effects in the single modulated diameter nanowire samples results in an intermediate width of the interaction field distribution with a localized convex decay. Thus, by a careful choice of methods of preparing high quality templates one can obtain complex magnetic nanowire systems with tunable magnetic properties. Furthermore, this study confirms that the FORC method is an effective tool for studying interactions and reversal properties of magnetic nanowire arrays.

ACKNOWLEDGMENTS

The financial support of the National Science Foundation (NSF) through Grant No. CCF-0403673 and ECCS-1028547 is acknowledged. The work in Suceava was supported by the project PRiDE, Contract no. POSDRU/89/1.5/S/57083 and the work in Iasi was supported by ANCS Grant PNII 12-093 HIFI and POSDRU/89/1.5/S/49944.

[1] A. Fert and L. Piraux, J. Magn. Magn. Mater. **200**, 338 (1999).
[2] R. Skomski, J. Phys.-Condes. Matter **15**, R841 (2003).
[3] D. J. Sellmyer, M. Zheng, and R. Skomski, J. Phys.-Condes. Matter **13**, R433 (2001).
[4] B. Ye, F. Li, D. Cimpoesu, J. B. Wiley, J. S. Jung, A. Stancu, and L. Spinu, J. Magn. Magn. Mater. **316**, E56 (2007).
[5] A. Mourachkine, O. V. Yazyev, C. Ducati, and J. P. Ansermet, Nano Lett. **8**, 3683 (2008).
[6] I. Huynen, G. Goglio, D. Vanhoenacker, and A. Vander Vorst, IEEE Microw. Guided Wave Lett. **9**, 401 (1999).
[7] S. Dubois, C. Marchal, J. M. Beuken, L. Piraux, J. L. Duvail, A. Fert, J. M. George, and J. L. Maurice, Appl. Phys. Lett. **70**, 396 (1997).
[8] R. A. Silva, T. S. Machado, G. Cernicchiaro, A. P. Guimaraes, and L. C. Sampaio, Phys. Rev. B **79**, 134434 (2009).
[9] N. Biziere, E. Mure, and J. P. Ansermet, Phys. Rev. B **79**, 012404 (2009).
[10] T. Maurer, F. Ott, G. Chaboussant, Y. Soumare, J. Y. Piquemal, and G. Viau, Appl. Phys. Lett. **91**, 3 (2007).
[11] T. L. Wade and J. E. Wegrowe, Eur. Phys. J.-Appl. Phys **29**, 3 (2005).
[12] C. R. Martin, Chem. Mater. **8**, 1739 (1996).
[13] R. L. Fleischer, P. B. Price, and R. M. Walker, *Nuclear tracks in solids : principles and applications* (University of California Press, Berkeley, 1975) pp. xxii, 605 p.
[14] R. Spohr, C. Zet, B. E. Fischer, H. Kiesewetter, P. Apel, I. Gunko, T. Ohgai, and L. Westerberg, Nucl. Instrum. Methods Phys. Res. Sect. B-Beam Interact. Mater. Atoms **268**, 676 (2010).
[15] H. Masuda and K. Fukuda, Science **268**, 1466 (1995).
[16] J. H. Lim, A. Rotaru, S. G. Min, L. Malkinski, and J. B. Wiley, J. Mater. Chem. **20**, 9246 (2010).
[17] A. Encinas-Oropesa, M. Demand, L. Piraux, I. Huynen, and U. Ebels, Phys. Rev. B **63**, 104415 (2001).
[18] A. Encinas-Oropesa, M. Demand, L. Piraux, U. Ebels, and I. Huynen, J. Appl. Phys. **89**, 6704 (2001).
[19] I. Dumitru, F. Li, J. B. Wiley, D. Cimpoesu, A. Stancu, and L. Spinu, IEEE Trans. Magn. **41**, 3361 (2005).
[20] O. C. Trusca, D. Cimpoesu, J. H. Lim, X. Zhang, J. B. Wiley, A. Diaconu, I. Dumitru, A. Stancu, and L. Spinu, IEEE Trans. Magn. **44**, 2730 (2008).
[21] J. Topp, D. Heitmann, and D. Grundler, Phys. Rev. B **80**, 174421 (2009).
[22] J. DeLaTorreMedina, L. Piraux, J. M. OlaisGovea, and A. Encinas, Phys. Rev. B **81**, 144411 (2010).
[23] T. G. Sorop, C. Untiedt, F. Luis, M. Kroll, M. Rasa, and L. J. de Jongh, Phys. Rev. B **67**, 014402 (2003).
[24] A. Sklyuyev, M. Ciureanu, C. Akyel, P. Ciureanu, and A. Yelon, J. Appl. Phys. **105**, 8 (2009).
[25] M. Hwang, M. Farhoud, Y. Hao, M. Walsh, T. A. Savas, H. I. Smith, and C. A. Ross, IEEE Trans. Magn. **36**, 3173 (2000).
[26] M. Bahiana, F. S. Amaral, S. Allende, and D. Altbir, Phys. Rev. B **74**, 174412 (2006).
[27] G. Bertotti, *Hysteresis in magnetism : for physicists, materials scientists, and engineers*, Electromagnetism (Academic Press, San Diego, 1998) pp. xvii, 558 p.
[28] I. D. Mayergoyz, *Mathematical models of hysteresis and their applications*, 1st ed., Elsevier series in electromagnetism, (Elsevier, Amsterdam ; Boston, 2003) pp. xxv, 472 p.
[29] G. W. D. Spratt, P. R. Bissell, R. W. Chantrell, and E. P. Wohlfarth, J. Magn. Magn. Mater. **75**, 309 (1988).
[30] P. E. Kelly, K. Ogrady, P. I. Mayo, and R. W. Chantrell, IEEE Trans. Magn. **25**, 3880 (1989).
[31] I. D. Mayergoyz, IEEE Trans. Magn. **22**, 603 (1986).

[32] C. R. Pike, A. P. Roberts, and K. L. Verosub, J. Appl. Phys. **85**, 6660 (1999).
[33] E. P. Wohlfarth, J. Appl. Phys. **29**, 595 (1958).
[34] F. Vajda, E. Della Torre, and R. D. McMichael, J. Appl. Phys. **75**, 5689 (1994).
[35] A. P. Roberts, C. R. Pike, and K. L. Verosub, J. Geophys. Res.-Solid Earth **105**, 28461 (2000).
[36] J. E. Davies, O. Hellwig, E. E. Fullerton, G. Denbeaux, J. B. Kortright, and K. Liu, Phys. Rev. B **70**, 224434 (2004).
[37] L. Spinu, A. Stancu, C. Radu, F. Li, and J. B. Wiley, IEEE Trans. Magn. **40**, 2116 (2004).
[38] J. E. Davies, O. Hellwig, E. E. Fullerton, J. S. Jiang, S. D. Bader, G. T. Zimanyi, and K. Liu, Appl. Phys. Lett. **86**, 3 (2005).
[39] J. E. Davies, J. Wu, C. Leighton, and K. Liu, Phys. Rev. B **72**, 134419 (2005).
[40] C. R. Pike, C. A. Ross, R. T. Scalettar, and G. Zimanyi, Phys. Rev. B **71**, 134407 (2005).
[41] H. G. Katzgraber, D. Herisson, M. Osth, P. Nordblad, A. Ito, and H. A. Katori, Phys. Rev. B **76**, 092408 (2007).
[42] R. K. Dumas, C. P. Li, I. V. Roshchin, I. K. Schuller, and K. Liu, Phys. Rev. B **75**, 134405 (2007).
[43] A. Stancu, D. Ricinschi, L. Mitoseriu, P. Postolache, and M. Okuyama, Appl. Phys. Lett. **83**, 3767 (2003).
[44] L. Stoleriu, A. Stancu, L. Mitoseriu, D. Piazza, and C. Galassi, Phys. Rev. B **74**, 174107 (2006).
[45] J. G. Ramirez, A. Sharoni, Y. Dubi, M. E. Gomez, and I. K. Schuller, Phys. Rev. B **79**, 235110 (2009).
[46] R. Tanasa, C. Enachescu, A. Stancu, J. Linares, E. Codjovi, F. Varret, and J. Haasnoot, Phys. Rev. B **71**, 014431 (2005).
[47] C. Enachescu, R. Tanasa, A. Stancu, F. Varret, J. Linares, and E. Codjovi, Phys. Rev. B **72**, 054413 (2005).
[48] M. M. Dirtu, C. Neuhausen, A. D. Naik, A. Rotaru, L. Spinu, and Y. Garcia, Inorg. Chem. **49**, 5723 (2010).
[49] A. Rotaru, J. Linares, F. Varret, E. Codjovi, A. Slimani, R. Tanasa, C. Enachescu, A. Stancu, and J. Haasnoot, Physical Review B **83**, 224107 (2011).
[50] F. Béron, L. Clime, M. Ciureanu, D. Ménard, R. W. Cochrane, and A. Yelon, IEEE Trans. Magn. **42**, 3060 (2006).
[51] L. Clime, S. Y. Zhao, F. Normandin, and T. Veres, J. Appl. Phys. **102**, 5 (2007).
[52] F. Béron, L. Clime, M. Ciureanu, D. Ménard, R. W. Cochrane, and A. Yelon, J. Appl. Phys. **101**, 3 (2007).
[53] F. Béron, L. P. Carignan, D. Ménard, and A. Yelon, IEEE Trans. Magn. **44**, 2745 (2008).
[54] R. Lavin, J. C. Denardin, J. Escrig, D. Altbir, A. Cortes, and H. Gomez, IEEE Trans. Magn. **44**, 2808 (2008).
[55] M. Ciureanu, F. Béron, P. Ciureanu, R. W. Cochrane, D. Ménard, A. Sklyuyev, and A. Yelon, J. Nanosci. Nanotechnol. **8**, 5725 (2008).
[56] T. R. F. Peixoto and D. R. Cornejo, J. Magn. Magn. Mater. **320**, E279 (2008).
[57] H. G. Katzgraber, F. Pazmandi, C. R. Pike, K. Liu, R. T. Scalettar, K. L. Verosub, and G. T. Zimanyi, Phys. Rev. Lett. **89**, 257202 (2002).
[58] R. J. Harrison and J. M. Feinberg, Geochem. Geophys. Geosyst. **9**, 11 (2008).
[59] D. X. Chen, J. A. Brug, and R. B. Goldfarb, IEEE Trans. Magn. **27**, 3601 (1991).
[60] R. Ferre, K. Ounadjela, J. M. George, L. Piraux, and S. Dubois, Phys. Rev. B **56**, 14066 (1997).
[61] R. Skomski, H. Zeng, M. Zheng, and D. J. Sellmyer, Phys. Rev. B **62**, 3900 (2000).
[62] M. Zheng, L. Menon, H. Zeng, Y. Liu, S. Bandyopadhyay, R. D. Kirby, and D. J. Sellmyer, Phys. Rev. B **62**, 12282 (2000).
[63] L. Sun, Y. Hao, C. L. Chien, and P. C. Searson, IBM J. Res. Dev. **49**, 79 (2005).